Decomposition-Based Design Optimization of Hybrid Electric Powertrain Architectures: Simultaneous Configuration and Sizing Design

Alparslan Emrah Bayrak
Mechanical Engineering,
University of Michigan,
Ann Arbor, MI 48109
e-mail: bayrak@umich.edu

Namwoo Kang[1]
Mechanical Engineering,
University of Michigan,
Ann Arbor, MI 48109
e-mail: nwkang@umich.edu

Panos Y. Papalambros
Mechanical Engineering,
University of Michigan,
Ann Arbor, MI 48109
e-mail: pyp@umich.edu

Effective electrification of automotive vehicles requires designing the powertrain's configuration along with sizing its components for a particular vehicle type. Employing planetary gear (PG) systems in hybrid electric vehicle (HEV) powertrain architectures allows various architecture alternatives to be explored, including single-mode architectures that are based on a fixed configuration and multimode architectures that allow switching power flow configuration during vehicle operation. Previous studies have addressed the configuration and sizing problems separately. However, the two problems are coupled and must be optimized together to achieve system optimality. An all-in-one (AIO) system solution approach to the combined problem is not viable due to the high complexity of the resulting optimization problem. This paper presents a partitioning and coordination strategy based on analytical target cascading (ATC) for simultaneous design of powertrain configuration and sizing for given vehicle applications. The capability of the proposed design framework is demonstrated by designing powertrains with one and two PGs for a midsize passenger vehicle. [DOI: 10.1115/1.4033655]

1 Introduction

Effective electrification of automotive powertrains requires solving the coupled topology and sizing design problem. Evaluation of design performance further depends on the control (or power management) strategy that distributes the power demand to the engine and motor/generators (MGs). HEV powertrain design is thus a challenging coupled physical (topology and size) and control (power management) system design problem. To complicate matters further, an HEV *configuration* is a connection scheme among powertrain components and the vehicle's output shaft(s), and some designs allow changing the configuration during vehicle operation using mechanical clutches (CLs). Each of these particular configurations is called the *driving mode* or simply *mode*. We define the collection of these modes (i.e., configurations) as the HEV *architecture*. The so-called power-split designs that can have a single-mode (see Fig. 1) or multimode architecture (see Fig. 2) connect the powertrain components to the vehicle output shaft in different ways using PG systems depending on the vehicle operational requirements. Existing architectures include one-PG [1,2], two-PG [3–7], and three-PG [8,9] architectures. In the remainder, we use the terms configuration, architecture, and mode as defined above and avoid using the term topology.

Configuration design has been studied in the literature in a broader perspective [10,11]. Effective design methodologies relying on a given library of components have been developed to generate and select configurations at the early design stages [12,13]. However, these methods are not applicable for detailed design of automotive powertrain architectures including component sizing and power management strategy.

A review of existing HEV powertrain design optimization strategies is given in Ref. [14]. Previous research in HEV powertrain design domain has focused on designing architectures for a given application and fixed powertrain component sizes and gear ratios [15–18]. Since feasible configurations define a disjoint design space, an AIO strategy cannot be used to solve the combined architecture and sizing problem. Here we formulate the combined optimal architecture, sizing, and controller design problem and employ the decomposition-based optimization strategy of ATC, to solve it. An earlier version of this work appeared in Ref. [19]. ATC is a hierarchical optimization methodology for multilevel systems [20,21] with proven convergence under certain assumptions [21] and demonstrated in industrial applications (e.g., Refs. [22] and [23]). Further generalization and computational improvement of ATC can be achieved using augmented Lagrangian relaxation for consistency [24]. A battery-HEV (BHEV) without plug-in capability will be used as a demonstration example.

The organization of the rest of the paper is as follows: Sec. 2 summarizes how architecture alternatives are created. Sec. 3 describes the formulation of the general HEV architecture optimization problem that combines configurations, sizing, and control using ATC. Sec. 4 presents results and discussion for the demonstration example and Sec. 5 offers conclusions.

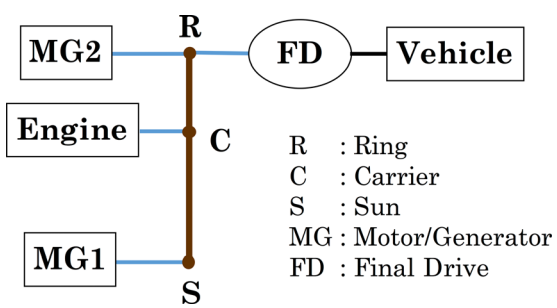

Fig. 1 Lever representation of a Toyota Prius like architecture

[1]Corresponding author.

Contributed by the Design Automation Committee of ASME for publication in the Journal of Mechanical Design. Manuscript received December 3, 2015; final manuscript received May 8, 2016; published online June 3, 2016. Assoc. Editor: Massimiliano Gobbi.

 Copyright © 2016 by ASME

Downloaded From: http://mechanicaldesign.asmedigitalcollection.asme.org/ on 06/03/2016 Terms of Use: http://www.asme.org/about-asme/terms-of-use

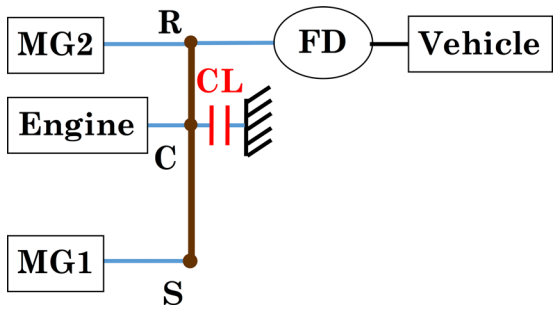

Fig. 2 Lever representation of a one-PG, dual-mode architecture with hybrid and pure-electric configurations

2 HEV Architecture Representation and Generation

We classify power-split architectures as single-mode, based on a fixed configuration, and multimode, consisting of multiple configurations. In this section, we describe a representation model for single- and multimode architectures and summarize the process to generate feasible powertrain configurations.

The "modified bond graph" model described in Refs. [17] and [25] is chosen to represent architecture decisions. Figure 3 shows the modified bond graph model corresponding to a Toyota Prius architecture shown in the lever analogy of Fig. 1. Vehicle output and powertrain components such as engine and MGs appear in every possible design candidate, so they are not design decisions and are represented by fixed "boxes." Each bond has its associated causal stroke and a bond weight (1, ρ, or $1+\rho$ where ρ is the PG ratio) that corresponds to a transformer modulus in the conventional bond graph representation. Connections among components through PGs are represented by bonds connected at "0" and "1" junctions. A 0-junction represents a constant power relationship where torques around the junction are the same and sum of the rotational speeds are equal to zero. A 1-junction also represents a constant power relationship with torque and speed relationships that of 0-junction are swapped. To explain the modified bond graph in Fig. 3, we describe the speed relationship it defines. The 0-junction along with the weights on the bonds represents the following kinematic relationship of a PG system:

$$(1+\rho)\omega_c = \rho\omega_r + \omega_s \tag{1}$$

where ω_r, ω_c, and ω_s denote the rotational speeds of ring, carrier, and sun gears, respectively. In this example, the engine is connected to the ring gear (represented by the bond around 0-junction with a weight of $1+\rho$) and MG1 is connected to the sun gear (the bond around 0-junction with a weight of 1). The 1-junction with three bonds binds the speeds of MG2 and the vehicle output shaft to be the same and equal to the speed of the ring gear (the bond around 0-junction with a weight of ρ). The final speed relationship can be summarized as follows:

$$\begin{bmatrix} 1+\rho & -\rho \\ 0 & 1 \end{bmatrix} \begin{bmatrix} \omega_{\text{eng}} \\ \omega_{\text{out}} \end{bmatrix} = \begin{bmatrix} \omega_{\text{MG1}} \\ \omega_{\text{MG2}} \end{bmatrix} \tag{2}$$

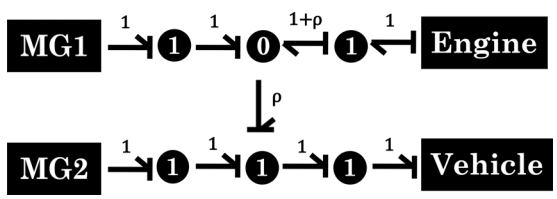

Fig. 3 Modified bond graph representation of the Toyota Prius architecture where ρ is the ring to sun PG ratio

where ω_{eng}, ω_{out}, ω_{MG1}, and ω_{MG2} denote the rotational speeds of the engine, output shaft, MG1, and MG2, respectively.

Using the modified bond graph representation, we generate all feasible configuration alternatives for a given set of powertrain components in a fully automated process. These configurations are used to create single- and multimode architectures. In this paper, we focus on a common case with an engine, two MGs, and a vehicle output shaft in one- and two-PG. The computation cost of generating all feasible configurations increases with the number of powertrain components. However, space and cost limitations do not allow this number to be so large in practice, making our generation process computationally tractable for practical cases.

2.1 Single-Mode Architecture. The single-mode architecture in Fig. 1 consists of a fixed configuration represented by a single modified bond graph, Fig. 3. In the BHEV example we use, there is no external charge source and so the architecture must sustain the battery state of charge (SOC) throughout the drive cycle, i.e., pure electric configurations without an engine are not considered feasible.

A 2×2 kinematic matrix denoted by $\mathbf{C}_{\text{mode}}$ is extracted from the modified bond graph representation to analyze the architecture. We define $\mathbf{C}_{\text{mode}}$ as

$$\mathbf{C}_{\text{mode}} \begin{bmatrix} \omega_{\text{eng}} \\ \omega_{\text{out}} \end{bmatrix} = \begin{bmatrix} \omega_{\text{MG1}} \\ \omega_{\text{MG2}} \end{bmatrix} \tag{3}$$

Using the input and output power equality, the torque relationships can be derived

$$-\mathbf{C}_{\text{mode}}^{-T} \begin{bmatrix} T_{\text{eng}} \\ -T_{\text{out}} \end{bmatrix} = \begin{bmatrix} T_{\text{MG1}} \\ T_{\text{MG2}} \end{bmatrix} \tag{4}$$

2.2 Multimode Architecture. The architecture shown in Fig. 2 is an example of a multimode architecture. When the CL is not engaged, the hybrid configuration is the same as that in Fig. 1. When the CL is engaged, the engine is connected to the ground (an immobile node) and a pure electric configuration is obtained. Pure electric configurations are feasible for multimode architectures as long as a hybrid mode exists.

We represent each particular configuration in a multimode architecture with a separate modified bond graph. Combination of two graphs represents the multimode architecture in this example. An additional step to calculate the number of CLs is needed when combining the configurations. A multimode architecture can be more complex with higher number of PGs and CLs such as the one by Ref. [6] in Fig. 4. The architecture in this figure has two hybrid modes obtained when (1) CL1 is engaged and CL2 disengaged, and (2) CL1 is disengaged and CL2 is engaged. For a given number of PGs, we use the number of CLs in the architecture as a complexity measure and use this measure to limit acceptable complexity in the generated architectures. As described in Ref. [18], the number of CLs needed can be calculated by comparing the modified bond graphs. When evaluating fuel economy and vehicle

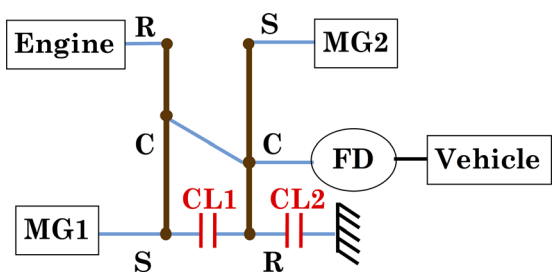

Fig. 4 Lever representation of a two-PG, dual-mode architecture with two hybrid configurations

Downloaded From: http://mechanicaldesign.asmedigitalcollection.asme.org/ on 06/03/2016 Terms of Use: http://www.asme.org/about-asme/terms-of-use

performance, hybrid configurations in multimode architectures can be analyzed in the same way as described in Sec. 2.1. The pure electric configuration in Fig. 2 is a kinematically 1-degree-of-freedom (DOF) configuration whose 2×2 kinematic matrix can be defined as follows:

$$\begin{bmatrix} 1 \\ 0 \end{bmatrix} \omega_{\text{out}} = \mathbf{C}_{\text{mode}} \begin{bmatrix} \omega_{\text{MG1}} \\ \omega_{\text{MG2}} \end{bmatrix} \tag{5}$$

A 2DOF pure electric configuration can be generated by defining its 1×2 kinematic matrix as

$$\omega_{\text{out}} = \mathbf{C}_{\text{mode}} \begin{bmatrix} \omega_{\text{MG1}} \\ \omega_{\text{MG2}} \end{bmatrix} \tag{6}$$

In evaluating performance or fuel consumption of a multimode architecture, the kinematic matrices shift when the mode is shifted.

2.3 Architecture Generation. The generation process has four main steps: (i) Given all powertrain components and number of PGs, the number of internal and external junctions is determined, and all possible simple and connected, undirected graphs are enumerated; (ii) for each undirected graph, junction types are assigned to the nodes and causal strokes obeying bond graph rules are assigned to the edges; (iii) bond weights representing the kinematic relationships among the gears of PG sets are assigned to the bonds; (iv) kinematic matrices described in Secs. 2.1 and 2.2 are extracted from the modified bond graphs for the analysis of the configurations. Details of the feasible configuration generation process are described in Ref. [17]. Only a brief summary of the results is presented here.

Using two MGs, one output shaft, one (optional) engine, and one (optional) ground, we generate 52 distinct feasible configurations for one PG, with 16 being hybrid and 36 being pure electric. Using the same set of powertrain components with two PGs, we generate 3420 feasible configurations with 2124 being hybrid and 1296 being pure electric. Some of these distinct two-PG configurations may have the same kinematic matrix. For instance, when both PG ratios are equal to 2, the 2124 hybrid configurations result in 1178 unique $\mathbf{C}_{\text{mode}}$ matrices. These kinematically equivalent designs can be useful for multimode designs; for example, with two kinematically equivalent configurations, we may select one with fewer CLs.

3 Generalized Architecture Design

The generalized architecture design problem involves selecting optimal powertrain configurations along with component sizes and a control strategy that minimize fuel consumption and satisfy performance constraints. We present the mathematical formulation of the combined problem and describe a solution strategy.

3.1 Problem Formulation. The mathematical formulation of the general architecture design problem is

$$\begin{aligned} &\min \quad f_{\text{cons}}(\mathbf{x}_c(N_{\text{mode}}), \mathbf{x}_s, \psi(t, \mathbf{x}_c(N_{\text{mode}}), \mathbf{x}_s, \mathbf{p})) \\ &\text{with respect to (w.r.t)} \\ &\quad \{\mathbf{x}_c(N_{\text{mode}}), \mathbf{x}_s, \psi(t, \mathbf{x}_c(N_{\text{mode}}), \mathbf{x}_s, \mathbf{p})\} \\ &\text{subject to (s.t.)} \\ &\quad \mathbf{g}_{\text{perf}}(\mathbf{x}_c(N_{\text{mode}}), \mathbf{x}_s, \psi(t, \mathbf{x}_c(N_{\text{mode}}), \mathbf{x}_s, \mathbf{p})) \le 0 \\ &\quad g_{\text{complex}}(\mathbf{x}_c(N_{\text{mode}})) \le 0 \\ &\quad \psi(t, \mathbf{x}_c(N_{\text{mode}}), \mathbf{x}_s, \mathbf{p}) \text{ is attainable} \\ &\quad \text{lb} \le \mathbf{x}_s \le \text{ub} \\ &\quad N_{\text{mode}} \in \{1, 2, 3, 4, ...\} \\ &\quad \mathbf{x}_c \text{ is feasible} \end{aligned} \tag{7}$$

The objective f_{cons} is the fuel consumption of the vehicle under a given set of drive cycles defined over time t. The objective depends on the configuration represented by a vector $\mathbf{x}_c$, the size of the powertrain components including gear ratios $\mathbf{x}_s$ (physical system design variables), the supervisory control policy ψ that distributes the demanded power to engine and MGs (control system design variable), and vehicle parameters $\mathbf{p}$ such as vehicle mass, wheel inertia, vehicle frontal area, and aerodynamic drag. Here, we focus on the case where $\mathbf{x}_s$ includes only the PG ratios and final drive ratio. Models for the engine, MGs, and battery with respect to their sizing variables can also be included in a more general case. The size of the vector $\mathbf{x}_c$ depends on the number of modes in the architecture denoted by N_{mode}.

The first set of constraints $\mathbf{g}_{\text{perf}}$ describes the performance requirements for the architecture including 0 to 60 miles per hour (mph) acceleration time, top speed, or gradeability. The next constraint denoted by g_{complex} is the complexity constraint measured by the number of CLs in the architecture as discussed in Sec. 2.2. The sizing variables are bounded by upper and lower bounds denoted by ub and lb, respectively. The control policy ψ must be attainable within the limits of the components and $\mathbf{x}_c$ must correspond to a feasible configuration.

3.2 Physical and Control System Design Problem. Several strategies have been proposed in the literature for the combined physical and control system design [26–28]. Solution strategies for this combined problem can be classified as *sequential*, *iterative*, *simultaneous,* and *nested* [29,30]. The sequential strategy assumes that the physical and control system design problems are fully separable and does not necessarily find the system optimum since it lacks the coupling term. The iterative strategy solves the physical and control system design problems multiple times in sequence until convergence, although convergence to the system optimum is not guaranteed. The simultaneous strategy is an AIO formulation successful examples of which include the design of passive dynamic systems with active control [27,31]. The nested strategy solves the control system design problem at each (external) physical system design iteration. Example implementations of nested strategy include Refs. [32] and [33]. Both strategies can achieve system optimality. The nested strategy is used here for simplicity. As discussed in Sec. 3.3, highly nonlinear nature of the physical system design problem itself with disjoint feasible design space makes the combined problem challenging. Even though simultaneous strategies appear as computationally efficient methods to solve combined physical and control system design problems, it will be further challenging to solve our problem with a simultaneous strategy that we leave to a future study.

The optimal control problem in the nested strategy that determines the optimal mode selection and distribution of the power demand to the powertrain components for minimizing fuel consumption is formulated as follows:

$$\begin{aligned} \min_{\omega_{\text{eng}}(t), T_{\text{eng}}(t), \gamma(t)} \quad & f_{\text{cons}} = \int_{t_0}^{t_f} \dot{m}_f\left(\omega_{\text{eng}}(t), T_{\text{eng}}(t), \gamma(t)\right) \cdot dt \\ \text{subject to} \quad & \boldsymbol{\omega}_{\min} \le \boldsymbol{\omega}(t) \le \boldsymbol{\omega}_{\max} \\ & \mathbf{T}_{\min} \le \mathbf{T}(t) \le \mathbf{T}_{\max} \\ & \gamma(t) \in \{1, 2, ..., N_{\text{mode}}\} \\ & \text{SOC}_{\min} \le \text{SOC}(t) \le \text{SOC}_{\max} \\ & \dot{\text{SOC}}(t) = f\left(\text{SOC}(t), \omega_{\text{eng}}(t), T_{\text{eng}}(t), \gamma(t)\right) \\ & \text{SOC}(t_0) = \text{SOC}(t_f) \end{aligned} \tag{8}$$

For a given powertrain design, the control objective is to minimize the total fuel consumption measured by integrating the fuel consumption rate denoted by $\dot{m}_f$ over the entire drive cycle, namely, from time t_0 to time t_f. Control variables are the engine operating points and the mode of the architecture denoted by γ. The constraints are bounds on the vectors $\boldsymbol{\omega}$ and $\mathbf{T}$ containing speeds and torques of engine and MGs on the mode signal to select one of the

Downloaded From: http://mechanicaldesign.asmedigitalcollection.asme.org/ on 06/03/2016 Terms of Use: http://www.asme.org/about-asme/terms-of-use

existing modes in the architecture and on the battery SOC. The constraint on $\dot{SOC}$ links the powertrain dynamics to the change in SOC. The final constraint sets the final SOC to the initial SOC and is specific to BHEV problems with no external charge source. The operating points $\boldsymbol{\omega}$ and $\mathbf{T}$ are related to each other through the kinematic matrix of the particular configuration in the architecture, as shown in Eqs. (3)–(6). Mode shifting in a multimode architecture switches this kinematic matrix. Solution of the optimal control problem in Eq. (8) gives the operating points of the powertrain components and the mode selection as a function of time.

Solving the control problem within the nested strategy can be achieved with dynamic programming [34,35], Pontryagin's minimum principle (PMP) [36,37], and equivalent consumption minimization strategy (ECMS) [38]. As discussed in Refs. [37] and [39], ECMS is not an optimal control strategy for general problems, but it can provide results close to the PMP with some simplified battery assumptions. Here, we use ECMS for its computational efficiency. ECMS implementation details are described in Ref. [25].

3.3 Problem Solution Via Decomposition. If $\mathbf{x}_c$ is represented by a modified bond graph, i.e., a vector consisting of adjacency matrix, junction types, causalities and weights on each bond, one approach is to define the elements of $\mathbf{x}_c$ as integer variables and $\mathbf{x}_s$ as continuous and solve the AIO problem using a derivative-free algorithm. However, not every modified bond graph corresponds to a feasible configuration. The feasibility

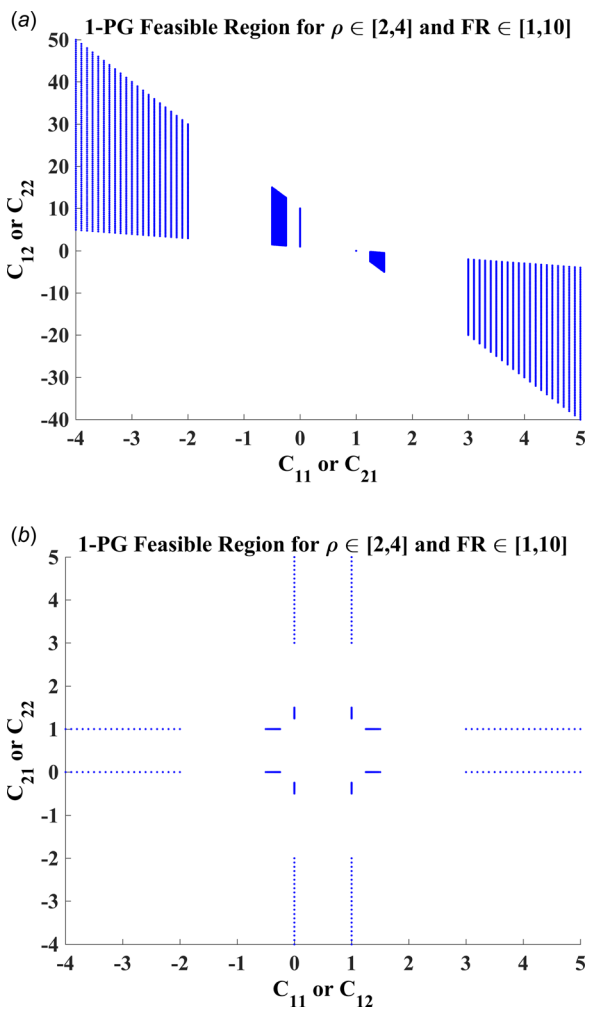

Fig. 5 Projection of the 4D feasible region of C_{conf} for one-PG hybrid designs to 2D planes. (*a*) C11 versus C12 (or C21 versus C22) and (*b*) C11 versus C21 (or C12 versus C22).

constraints on $\mathbf{x}_c$ define a very small and disjoint design space, and derivative-free methods do not work. We can enumerate all feasible configurations to create a feasible design space for $\mathbf{x}_c$ and optimize $\mathbf{x}_s$ for each feasible configuration. The nested control problem is computationally expensive, and so enumeration can work for a small number of feasible configurations such as for one-PG single-mode architectures with 16 feasible configurations.

An alternative representation uses continuous variables for both configuration and sizing. The kinematic relationship matrix $\mathbf{C}_{\text{mode}}$ introduced in Sec. 2 depends on both configuration and PG ratios. To include the final drive ratio, we define

$$\mathbf{C}_{\text{conf}}(\mathbf{x}_c, \mathbf{x}_s) = \begin{cases} \mathbf{C}_{\text{mode}} \cdot \begin{bmatrix} 1 & 0 \\ 0 & \text{FR} \end{bmatrix} & \text{if hybrid mode} \\ \mathbf{C}_{\text{mode}} \cdot 1/\text{FR} & \text{if pure electric mode} \end{cases} \tag{9}$$

where $\mathbf{x}_s = \begin{bmatrix} \boldsymbol{\rho}; & \text{FR} \end{bmatrix}$, $\boldsymbol{\rho}$ is the vector of PG ratios and FR is the final drive ratio. The elements of $\mathbf{C}_{\text{conf}}$ can be optimized to minimize fuel consumption with vehicle performance constraints as proposed by Cheong et al. [40]. However, contrary to the case discussed by Cheong et al., not all $\mathbf{C}_{\text{conf}}$ matrices correspond to feasible configurations. For example, Fig. 5 shows the projections of four-dimensional feasible design space of $\mathbf{C}_{\text{conf}}$ elements onto two-dimensional planes for one-PG hybrid modes. The empty regions in the design space correspond to infeasible configurations.

Defining constraints for $\mathbf{C}_{\text{conf}}$ feasibility becomes complicated as the number of PGs increases. For a general formulation accounting for feasibility, we introduce partitions for single-mode and multimode design subproblems and use ATC to coordinate them. The general ATC subproblem P_{ij} corresponding to the jth element at the ith level is

$$\begin{aligned} &\min \ f_{ij}(\bar{\mathbf{x}}_{ij}) + \phi(\mathbf{c}) \\ &\text{w.r.t.} \ \bar{\mathbf{x}}_{ij} = \left[\mathbf{x}_{ij}; \mathbf{t}_{(i+1)k_1}; \ldots; \mathbf{t}_{(i+1)k_{n_{c_{ij}}}}\right] \\ &\text{s.t.} \ \mathbf{g}_{ij}(\bar{\mathbf{x}}_{ij}) \le 0 \\ &\quad \mathbf{h}_{\text{ij}}(\bar{\mathbf{x}}_{\text{ij}}) = 0 \\ &\text{where } \mathbf{c} = \left[(\mathbf{t}_{ij} - \mathbf{r}_{ij}); (\mathbf{t}_{(i+1)k_1} - \mathbf{r}_{(i+1)k_1}); \ldots; \left(\mathbf{t}_{(i+1)k_{n_{c_{ij}}}} - \mathbf{r}_{(i+1)k_{n_{c_{ij}}}}\right)\right] \\ &\quad \phi(\mathbf{c}) = \mathbf{v}^T(\mathbf{c}) + \|\mathbf{w} \circ \mathbf{c}\|_2^2 \end{aligned} \tag{10}$$

Here, f_{ij} is the local objective function, $\bar{\mathbf{x}}_{ij}$ is the vector of optimization variables, $\mathbf{x}_{ij}$ is the vector of local design variables, $\mathbf{g}_{ij}$ and $\mathbf{h}_{ij}$ are the local inequality and equality constraints, respectively, $\mathbf{t}_{ij}$ is the vector of children target optimization variables, $\mathbf{r}_{ij}$ is the vector of local element responses, $n_{c_{ij}}$ is the number of children, $\mathbf{c}$ is the vector of inconsistencies between targets and responses, and ϕ is a penalty function.

The ATC-augmented Lagrangian penalty function formulation with alternating direction method of multipliers [24] is used, where $\mathbf{v}$ is the vector of Lagrange multipliers, $\mathbf{w}$ is the vector of quadratic penalty weights, and the Hadamard symbol $\circ$ is used to denote term-by-term multiplication of vectors. After solving all subproblems of iteration k, the penalty weights are updated according to

$$\mathbf{w}^{k+1} = \beta \mathbf{w}^k \tag{11}$$

where $\beta \ge 1$, typically selecting $2 < \beta < 3$. The Lagrange multiplier estimates are updated as

$$\mathbf{v}^{k+1} = \mathbf{v}^k + 2\ \mathbf{w}^k \circ \mathbf{w}^k \circ \mathbf{c}^k \tag{12}$$

Two termination criteria are used: The change in the maximal consistency constraint value after two consecutive iterations must be smaller than a positive threshold ε_1

Downloaded From: http://mechanicaldesign.asmedigitalcollection.asme.org/ on 06/03/2016 Terms of Use: http://www.asme.org/about-asme/terms-of-use

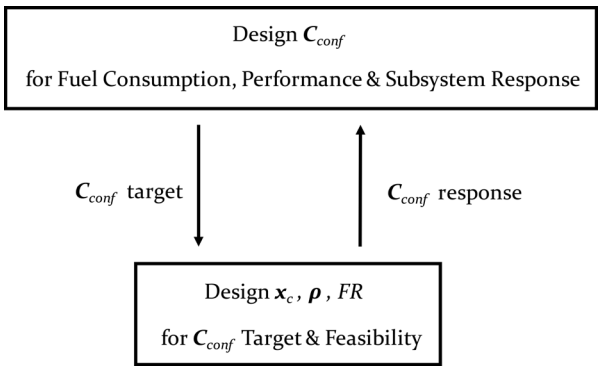

Fig. 6 Decomposition of combined single-mode architecture and gear ratio design

$$\|\mathbf{c}^k - \mathbf{c}^{k-1}\|_\infty < \varepsilon_1 \tag{13}$$

and the maximal consistency constraint violation must be smaller than a positive threshold ε_2

$$\|\mathbf{c}^k\|_\infty < \varepsilon_2 \tag{14}$$

3.3.1 Single-Mode Architecture Design. The problem partitioning for single-mode architecture design is shown in Fig. 6. The system level solves the fuel consumption minimization problem with respect to $\mathbf{C}_{\text{conf}}$, considering vehicle performance and subsystem response. The system problem does not consider feasibility of $\mathbf{C}_{\text{conf}}$. The system-level solution is sent to the subsystem level as a target. The subsystem-level problem tries to meet this target as close as possible by designing gear ratios for feasible configurations.

The system-level problem is formulated as follows:

$$\begin{aligned}
\min\quad & f_{\text{cons}}\left(\mathbf{C}^U_{\text{conf}}, \psi^*\left(t, \mathbf{C}^U_{\text{conf}}, \mathbf{p}\right)\right) + \phi\left(\mathbf{C}^U_{\text{conf}} - \mathbf{C}^L_{\text{conf}}\right)\\
\text{w.r.t.}\quad & [C_{11}; C_{12}; C_{21}; C_{22}], \text{ where } \mathbf{C}^U_{\text{conf}} = \begin{bmatrix} C_{11} & C_{12} \\ C_{21} & C_{22} \end{bmatrix}\\
\text{s.t.}\quad & \mathbf{g}_{\text{perf}}\left(\mathbf{C}^U_{\text{conf}}, \psi^*\left(t, \mathbf{C}^U_{\text{conf}}, \mathbf{p}\right)\right) \le 0\\
& \text{lb} \le \mathbf{C}^U_{\text{conf}} \le \text{ub}\\
& |\det\left(\mathbf{C}^U_{\text{conf}}\right)| > 0
\end{aligned} \tag{15}$$

where ϕ is the augmented Lagrangian penalty function [24]. Superscripts $(\cdot)^U$ and $(\cdot)^L$ indicate upper and lower system variables, respectively, and ψ^* denotes the optimal control strategy obtained by solving a nested control problem. The elements of $\mathbf{C}_{\text{conf}}$ are continuous design variables and all invertible $\mathbf{C}_{\text{conf}}$ are assumed to be feasible. A 2DOF hybrid configuration must have a nonsingular $\mathbf{C}_{\text{conf}}$. So, we include invertibility as a constraint at the system level. The optimal $\mathbf{C}_{\text{conf}}$ obtained by the system-level problem is passed to the subsystem level as a target. The subsystem-level problem addresses feasibility of $\mathbf{C}_{\text{conf}}$ based on the feasible configurations generated earlier. The subsystem-level problem is stated as follows:

$$\begin{aligned}
\min\quad & \phi\left(\mathbf{C}^U_{\text{conf}} - \mathbf{C}^L_{\text{conf}}\right)\\
\text{w.r.t.}\quad & \mathbf{x} = [\mathbf{x}_c; \mathbf{x}_s], \text{ where } \mathbf{x}_s = [\boldsymbol{\rho}; \text{FR}]\\
\text{s.t.}\quad & \text{lb} \le \mathbf{x}_s \le \text{ub}\\
& \mathbf{x}_c \text{ is feasible}\\
& \mathbf{C}^L_{\text{conf}} = f_{\text{conf}}(\mathbf{x})
\end{aligned} \tag{16}$$

where f_{conf} is the function that maps the configuration and gear ratios to the kinematic relationship matrix. This function processes the bond graph representation of the configuration and uses the gear ratio values to obtain 2×2 kinematic relationship matrix. See Refs. [17] and [25] for details of this process. We solve this problem with respect to $\mathbf{x}_s$ for all feasible $\mathbf{x}_c$ separately and select the set of $\mathbf{x} = [\mathbf{x}_c; \mathbf{x}_s]$ that meets the target the best. Since the subsystem-level problem does not involve controls, evaluation of f_{conf} is almost instantaneous and computational cost is very low.

3.3.2 Multimode Architecture Design. In the multimode architecture design, the main partitioning idea remains the same. However, the system- and subsystem-level formulations slightly differ from the single-mode design. Problem partitioning is depicted in Fig. 7. The number of subsystems is equal to the number of modes to be designed. As seen in Fig. 7, the sizing variables are shared among subsystems. The design variables of the system-level problem are the elements of the $\mathbf{C}_{\text{conf}}$ matrix of all the modes in the architecture and sizing variables. The objective of the system-level problem has an additional penalty on the difference between targets and responses for these shared variables. The complexity constraint mentioned earlier appears in each subsystem. The formulation for the system-level problem is

$$\begin{aligned}
\min\quad & f_{\text{cons}}\left(\mathbf{C}^U_{\text{conf},i}, \psi^*\left(t, \mathbf{C}^U_{\text{conf},i}, \mathbf{p}\right)\right)\\
& + \sum_{i=1}^{N_{\text{mode}}} \phi\left(\mathbf{C}^U_{\text{conf},i} - \mathbf{C}^L_{\text{conf},i}\right) + \phi\left(\mathbf{x}^U_s - \mathbf{x}^L_{s,i}\right)\\
\text{w.r.t.}\quad & \left[C_{11,i}; C_{12,i}; C_{21,i}; C_{22,i}; \mathbf{x}^U_s\right],\\
\text{where}\quad & \mathbf{C}^U_{\text{conf},i} = \begin{bmatrix} C_{11,i} & C_{12,i} \\ C_{21,i} & C_{22,i} \end{bmatrix} \forall i \in \{1, \ldots N_{\text{mode}}\}\\
\text{s.t.}\quad & \mathbf{g}_{\text{perf}}\left(\mathbf{C}^U_{\text{conf},i}, \psi^*\left(t, \mathbf{C}^U_{\text{conf},i}, \mathbf{p}\right)\right) \le 0\\
& \text{lb}_i \le \mathbf{C}^U_{\text{conf},i} \le \text{ub}_i\\
& |\det\left(\mathbf{C}^U_{\text{conf},i}\right)| > 0_i
\end{aligned} \tag{17}$$

where the subscript $(\cdot)_{,i}$ denotes each individual mode in the architecture. Each $\mathbf{C}_{\text{conf},i}$ optimized at the system level is sent as target to the corresponding subsystems. Also, the same $\mathbf{x}_s$ is sent to every subsystem as it is the vector of shared variables. The formulation for a subsystem i becomes

$$\begin{aligned}
\min\quad & \phi\left(\mathbf{C}^U_{\text{conf},i} - \mathbf{C}^L_{\text{conf},i}\right) + \phi\left(\mathbf{x}^U_s - \mathbf{x}^L_{s,i}\right)\\
\text{w.r.t.}\quad & \mathbf{x}_i = \left[\mathbf{x}_{c,i}; \mathbf{x}^L_{s,i}\right], \text{ where } \mathbf{x}^L_{s,i} = [\boldsymbol{\rho}_i; \text{FR}_i]\\
\text{s.t.}\quad & g_{\text{complex}}(\mathbf{x}_{c,i}, \mathbf{x}_{c,j}) \le 0 \quad \forall j \in \{1, \ldots N_{\text{mode}} | j \ne i\}\\
& \text{lb}_i \le \mathbf{x}^L_{s,i} \le \text{ub}_i\\
& \mathbf{x}_{c,i} \text{ is feasible}\\
& \mathbf{C}^L_{\text{conf},i} = f_{\text{conf}}(\mathbf{x}_i)
\end{aligned} \tag{18}$$

4 Results and Discussion

In this section, we present a case study to demonstrate the application of the proposed method to the powertrain design of a mid-size vehicle. Key specifications for the vehicle and powertrain components used in the BHEV example are listed in Table 1. In this case study, we calculate the power demand from the powertrain assuming that the vehicle follows the drive cycle exactly. We add rolling resistance and aerodynamic drag to the demand from the drive cycle.

We use a static battery model that neglects the battery transients to calculate battery losses and SOC. We simplify the model by assuming fixed battery output voltage and efficiency. In the

Downloaded From: http://mechanicaldesign.asmedigitalcollection.asme.org/ on 06/03/2016 Terms of Use: http://www.asme.org/about-asme/terms-of-use

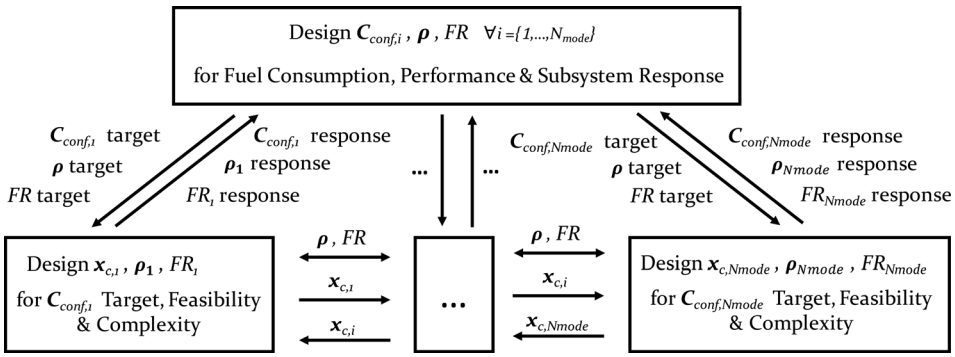

Fig. 7 Decomposition of combined multimode architecture and gear ratio design

Table 1 Vehicle specifications used for the case studies

Specification	Value
Vehicle body mass	1400 kg
Tire radius	0.3 m
Aerodynamic drag coefficient	0.29
Frontal area	2 m^2
Battery voltage	350 V
Battery efficiency	92%
Battery capacity	6.5 A h
Rated MG1 power	42 kW
Rated MG2 power	60 kW
Max. MG speed	12,000 rpm
Max. MG torque	200 N · m
Rated engine power	43 kW
Max. engine torque	102 N · m
Engine displacement size	1.5 L

control problem, we allow the battery SOC to vary between 40% and 80%. We set a battery maximum charging current limit of 100 A to limit the regenerative braking power. Models for the MGs rely on efficiency maps and maximum/minimum torque maps. We use these maps to calculate the motor loss and current input to the battery model. We assume a fixed inverter efficiency of 95% that is integrated in the efficiency map. Similarly, the engine model uses a fuel consumption map with respect to engine torques and speeds. A maximum engine torque curve as a function of engine speed limits the output torque of the engine.

Fuel economy f_{mpg} is calculated using the average of city (the Urban Dynamometer Driving Schedule) and highway (the Highway Fuel Economy Test) cycle consumptions. The control problem is solved with nested strategy and ECMS as described in Sec. 3.2. Acceleration time t_{60mph} must be less than 12 s and top speed V_{top} at least 105 mph. PG ratios vary between 2 and 4 and final drive ratio between 1 and 10.

ATC allows using different optimizers for each subproblem. A genetic algorithm (GA) solves the system-level and sequential quadratic programming (SQP) combined with enumeration of all feasible configurations to solve the subsystem-level problems. When the problem is partitioned as described in Sec. 3.3, tests showed that the system-level problem is highly dependent on the initial population selection due to the disjoint nature of the design space. Thus, we generate some feasible designs from each configuration and randomly select among them to provide an initial population to the GA. To improve the convergence of GA during ATC iterations, we set initial populations based on optimization results from the previous iteration. At every iteration, we randomly select half of the population from the best (feasible) results from subsystems and set remaining populations randomly. For a given configuration $\mathbf{x}_c$, the subsystem-level problem can be expressed analytically by extracting the $\mathbf{C}_{conf}$ matrices from the modified bond graph representation and quickly solved with SQP. We use $\varepsilon_1 = \varepsilon_2 = 0.01$ for all problems. We set ε values by checking perturbation values of $\mathbf{C}_{conf}$ that produce the same vehicle performance. The convergence of ATC is also affected by the choice of βs that represent the weights between local objective function (exploration) and penalty function (convergence). We tested different β values between 1 and 3 to find a beta value for each architecture case that well balances the objective and penalty functions. We set $\beta = 1.25$ for the results in Secs. 4.1–4.3 and set $\beta = 1.75$ for the results in Sec. 4.4. Our seeding strategy with proper β values yields a smooth convergence between target and response. For the largest problem considered in this paper (multimode two-PG design), one ATC iteration of a GA run at the upper level takes approximately 1 hr on average using parallel computing on an Intel Xeon E5-2620 v2 at 2.10 GHz CPU and 128 GB RAM, while SQP in lower level takes approximately 5 min on average.

4.1 Single-Mode One-PG Architecture Results. Before implementing the ATC process, we first optimize all 16 configurations using SQP and starting from different initial gear ratio selections and select the best one, see Table 2. We take these optimal results as a reference point when evaluating ATC solutions.

Table 2 Single-mode one-PG architecture design results for optimizing each configuration separately

Initial $\begin{bmatrix}\rho_0\\ FR_0\end{bmatrix}$	Optimal $\begin{bmatrix}\rho^*\\ FR^*\end{bmatrix}$	Optimal $\mathbf{C}_{conf}$	f_{mpg} (mpg)	V_{top} (mph)	t_{60mph} (s)
$\begin{bmatrix}2\\1.5\end{bmatrix}$	$\begin{bmatrix}2.01\\4.27\end{bmatrix}$	$\begin{bmatrix}3.01 & -8.59\\0 & 4.27\end{bmatrix}$	56.81	108	11.66
$\begin{bmatrix}2.5\\2.5\end{bmatrix}$	$\begin{bmatrix}2.00\\4.25\end{bmatrix}$	$\begin{bmatrix}3.00 & -8.50\\0 & 4.29\end{bmatrix}$	56.80	108	11.74
$\begin{bmatrix}3\\3.5\end{bmatrix}$	$\begin{bmatrix}2.00\\4.29\end{bmatrix}$	$\begin{bmatrix}3.00 & -8.57\\0 & 4.29\end{bmatrix}$	56.87	108	11.64

Table 3 ATC results for single-mode one-PG architecture design using GA with five generations for the system-level problem

Optimal $\mathbf{C}_{conf}$	Optimal $\mathbf{x}_s$	f_{mpg} (mpg)	V_{top} (mph)	t_{60mph} (s)
$\begin{bmatrix}3.67 & -11.46\\0 & 4.28\end{bmatrix}$	$\rho^* = 2.67$ $FR^* = 4.28$	56.37	111	10.73
$\begin{bmatrix}3.84 & -12.00\\0 & 4.21\end{bmatrix}$	$\rho^* = 2.85$ $FR^* = 4.21$	56.24	111	11.98
$\begin{bmatrix}4.07 & -11.58\\0 & 3.77\end{bmatrix}$	$\rho^* = 3.07$ $FR^* = 3.77$	56.35	109	11.57

Downloaded From: http://mechanicaldesign.asmedigitalcollection.asme.org/ on 06/03/2016 Terms of Use: http://www.asme.org/about-asme/terms-of-use

The results in Table 2 are close. For some solutions, the PG ratio lower bound is active. Relaxing the bound is limited by PG design practicality. The smallest pinion gear size limits the PG ratio to 2 in practice [41]. The architecture corresponding to these results is the same as the one-PG architecture of the Toyota Prius shown in Fig. 1.

When solving the problem given in Sec. 3.3.1 for one-PG configuration, we provide feasible initial populations selected randomly from the pool of feasible designs generated from each configuration for the system-level problem. In order to ensure variety, we select designs from each feasible configuration. We set the population size to 100 and select three sets of populations. The ATC process converges after 11, 21, and 8 iterations for each of the three initial populations, respectively. The results are shown in Table 3.

The configurations are all the same as the one in Fig. 1. The GA results are consistent and close to the results obtained from optimizing each configuration one by one. Both approaches converge to the same configuration with some difference in the gear ratios. After ATC converges, we can employ a local search on the gear ratios using the final configuration to fine-tune the results. The number of necessary generations depends on the problem. In this case, it was empirically set to 5. Increasing the generation number does not show significant improvement in the results [25].

4.2 Single-Mode Two-PG Architecture Results. When we increase the number of PGs in the architecture, the system-level problem does not change, but the subsystem-level problem has more design variables and more configurations to search. Due to the complexity of the problem, the exhaustive enumeration used to validate the results of the proposed method in the one-PG case is not possible in two-PG case but we can use the lessons learned from the one-PG study to increase the chance of finding good designs. For example, in the one-PG case, the system-level solution is affected by the initial population selection due to the disjoint feasible space; to reduce this effect, we provide a variety of configurations in the initial population. When selecting initial population, we have more than 100 feasible configurations in this case. We can group the designs based on the sign of the elements of $\mathbf{C}_{\text{conf}}$ matrix. Since this matrix has four elements and each element can be either positive, negative, or zero, we have 81 possible types of $\mathbf{C}_{\text{conf}}$ matrices. Selecting randomly 100 designs in total from each of these groups, we tested three initial populations. ATC converged after 4, 3, and 3 iterations for the three initial populations, respectively. Table 4 shows the results for this case.

The computations consistently converged to similar optimal designs and the configuration corresponding to these $\mathbf{C}_{\text{conf}}$ matrices is shown in Fig. 8.

4.3 Dual-Mode One-PG Architecture Results. We solve the multimode architecture design problem formulated in Sec. 3.3.2 for two modes using one-PG configurations with the same settings as before. ATC converged after 27, 9, and 25 iterations for the three initial populations, respectively, see Table 5. Three initial populations with similar optimal results converged to the dual-mode architecture depicted in Fig. 2.

Table 4 ATC results for single-mode two-PG architecture design using GA with five generations for the system-level problem

Optimal $\mathbf{C}_{\text{conf}}$	Optimal $\mathbf{x}_s$	f_{mpg} (mpg)	V_{top} (mph)	$t_{60\text{mph}}$ (s)
$\begin{bmatrix} 4.33 & -11.48 \\ 0 & 4.62 \end{bmatrix}$	$\rho_1^* = 3.33$ $\rho_2^* = 2.94$ $\text{FR}^* = 3.44$	57.56	105	11.44
$\begin{bmatrix} 4.56 & -11.94 \\ 0 & 4.5 \end{bmatrix}$	$\rho_1^* = 3.55$ $\rho_2^* = 2.94$ $\text{FR}^* = 3.35$	57.51	105	11.52
$\begin{bmatrix} 3.98 & -11.28 \\ 0 & 5.33 \end{bmatrix}$	$\rho_1^* = 2.45$ $\rho_2^* = 2.98$ $\text{FR}^* = 3.78$	57.81	105	10.65

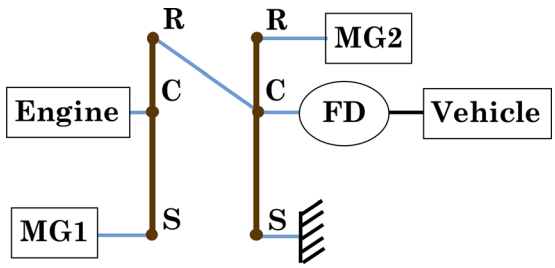

Fig. 8 Optimal single-mode two-PG architecture obtained by ATC

4.4 Multimode Two-PG Architecture results. We solve the multimode architecture design problem for two modes using two-PG configurations. Since the number of possible architectures is much larger compared to the previous cases, we increase the initial population size to 300 in order to provide more variety. Larger population size brings a trade-off between finding possibly better solutions and higher computational cost. In the previous cases, increasing the population size from 100 to larger values does not yield any substantial improvement in the results, while in this case gradually increasing the population size from 100 to 300 keeps improving the final optimization results. Here, we show the results with three initial populations of size 300. ATC converged after 12, 12, and 27 iterations for the three initial populations, respectively, see Table 6. Two of these optimization runs converged to the same architecture but the last results converged to the infeasible design with a different architecture violating 0–60 mph acceleration time constraint. The violated constraint is highlighted in bold. The optimal architecture obtained in the first two optimization runs is shown in Fig. 9. These results show that this case is more sensitive to the initial population selection. Considering the

Table 5 ATC results for dual-mode one-PG architecture design using GA with five generations for the system-level problem

Optimal $\mathbf{C}_{\text{conf},1}$	Optimal $\mathbf{C}_{\text{conf},2}$	Optimal $\mathbf{x}_s$	f_{mpg} (mpg)	V_{top} (mph)	$t_{60\text{mph}}$ (s)
$\begin{bmatrix} 3.00 & -9.37 \\ 0 & 4.68 \end{bmatrix}$	$\begin{bmatrix} 0 & -0.21 \\ 0.21 & 0.43 \end{bmatrix}$	$\rho^* = 2.00$ $\text{FR}^* = 4.68$	58.46	110	7.09
$\begin{bmatrix} 3.08 & -10.25 \\ 0 & 4.92 \end{bmatrix}$	$\begin{bmatrix} 0 & -0.20 \\ 0.20 & 0.41 \end{bmatrix}$	$\rho^* = 2.08$ $\text{FR}^* = 4.93$	59.97	112	7.04
$\begin{bmatrix} 3.03 & -9.60 \\ 0 & 4.72 \end{bmatrix}$	$\begin{bmatrix} 0 & -0.21 \\ 0.21 & 0.43 \end{bmatrix}$	$\rho^* = 2.03$ $\text{FR}^* = 4.72$	58.83	111	7.11

Table 6 ATC results for dual-mode two-PG architecture design using GA with five generations for the system-level problem

Optimal $\mathbf{C}_{\text{conf},1}$	Optimal $\mathbf{C}_{\text{conf},2}$	Optimal $\mathbf{x}_s$	f_{mpg} (mpg)	V_{top} (mph)	$t_{60\text{mph}}$ (s)
$\begin{bmatrix} -0.50 & 5.63 \\ -0.34 & 5.04 \end{bmatrix}$	$\begin{bmatrix} 0 & -0.20 \\ 0.26 & -0.30 \end{bmatrix}$	$\rho_1^* = 2.17$ $\rho_2^* = 2.00$ $\text{FR}^* = 3.75$	75.22	108	7.12
$\begin{bmatrix} -0.60 & 5.91 \\ -0.40 & 5.16 \end{bmatrix}$	$\begin{bmatrix} 0 & -0.18 \\ 0.27 & -0.31 \end{bmatrix}$	$\rho_1^* = 2.48$ $\rho_2^* = 2.00$ $\text{FR}^* = 3.68$	73.79	106	6.87
$\begin{bmatrix} -2.79 & 6.77 \\ 7.40 & -11.44 \end{bmatrix}$	$\begin{bmatrix} 0 & 0.09 \\ 0.56 & 0.33 \end{bmatrix}$	$\rho_1^* = 2.65$ $\rho_2 * = 2.79$ $\text{FR}^* = 1.78$	56.38	117	**27.81**

Downloaded From: http://mechanicaldesign.asmedigitalcollection.asme.org/ on 06/03/2016 Terms of Use: http://www.asme.org/about-asme/terms-of-use

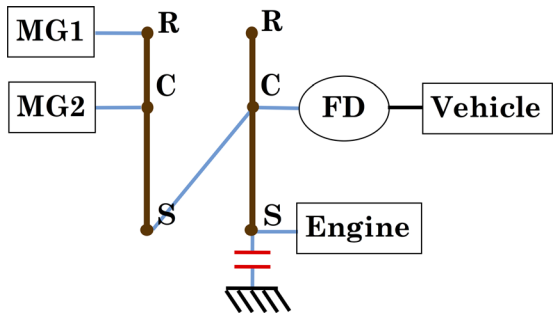

Fig. 9 Optimal two-PG dual-mode obtained by ATC

number of possible architecture candidates for this case, such sensitivity is expected. The dependency of the results on the initial population can be reduced by further increasing the initial population size and generation number, which can potentially improve the final results.

The results we present in this section show an improvement trend as the number of PGs and the number of modes in the architecture increase. However, that increase also comes with additional cost and space requirements. Overall, the decision on the final architecture for a given application must be considered with the cost and space limitation.

5 Conclusion and Future Work

We proposed a formulation and an ATC-based strategy to address the combined optimal HEV architecture, sizing, and control problem. We solved the system-level problem using a specially seeded GA and the subsystem-level problems using SQP. We demonstrated the framework with a BHEV example for a midsize passenger vehicle. Different initial populations consistently converged to the same architecture with some variations in the gear ratios in each case.

The variation in the optimal gear ratios from the optimization runs with different initial populations can be eliminated by performing an additional local search on the gear ratios after ATC converges. As shown in Table 2, optimizing only the gear ratios gives consistently similar optimal results. However, optimizing the gear ratios for all feasible configurations would not be tractable for a problem with too many feasible configurations. Therefore, having an optimal configuration from ATC can be used as a good initial guess for an additional local search to improve results further. The formulation is general enough to include size variables for other components such as engine, MG, and battery. Adding these variables will increase not only the computational complexity but also the range of decisions that can be included in the architecture system optimization problem.

The configuration design strategy presented in this article is clearly tailored to the particular HEV domain. We believe that the modified bond graph concept and the modeling and solution approach followed to link topology, sizing, and control problems can be used for other electromechanical system design problems, but we believe that such use will be also application specific. True generalization to all electromechanical systems remains an open question.

Acknowledgment

This research has been partially supported by General Motors Corp., the Automotive Research Center, a U.S. Army Center of Excellence at the University of Michigan, and a University of Michigan Graham Sustainability Institute Fellowship. This support is gracefully acknowledged.

References

[1] Conlon, B. M., Savagian, P. J., Holmes, A. G., and Harpster, M. O., 2011, "Output Split Electrically-Variable Transmission With Electric Propulsion Using One or Two Motors," U.S. Patent No. 7,867,124.
[2] Sasaki, S., 1998, "Toyota's Newly Developed Hybrid Powertrain," 10th International Symposium on Power Semiconductor Devices and ICs, IEEE, pp. 17–22.
[3] Schmidt, M., 1996, "Two-Mode, Input-Split, Parallel, Hybrid Transmission," U.S. Patent No. 5,558,588.
[4] Schmidt, M., 1996, "Two-Mode, Split Power, Electro-Mechanical Transmission," U.S. Patent No. 5,577,973.
[5] Holmes, A., Klemen, D., and Schmidt, M., 2003, "Electrically Variable Transmission With Selective Input Split, Compound Split, Neutral and Reverse Modes," U.S. Patent No. 6,527,658.
[6] Holmes, A., and Schmidt, M., 2002, "Hybrid Electric Powertrain Including a Two-Mode Electrically Variable Transmission," U.S. Patent No. 6,478,705.
[7] Ai, X., and Anderson, S., 2005, "An Electro-Mechanical Infinitely Variable Transmission for Hybrid Electric Vehicles," SAE Technical Paper No. 2005-01-0281.
[8] Schmidt, M., 1999, "Two-Mode, Compound-Split Electro-Mechanical Vehicular Transmission," U.S. Patent No. 5,931,757.
[9] Raghavan, M., Bucknor, N. K., and Hendrickson, J. D., 2007, "Electrically Variable Transmission Having Three Interconnected Planetary Gear Sets, Two Clutches and Two Brakes," U.S. Patent No. 7,179,187.
[10] Chakrabarti, A., Shea, K., Stone, R., Cagan, J., Campbell, M., Hernandez, N. V., and Wood, K. L., 2011, "Computer-Based Design Synthesis Research: An Overview," J. Comput. Inf. Sci. Eng., **11**(2), p. 021003.
[11] Crawley, E., Cameron, B., and Selva, D., 2015, *System Architecture: Strategy and Product Development for Complex Systems*, Prentice Hall, Upper Saddle River, NJ.
[12] Campbell, M. I., Cagan, J., and Kotovsky, K., 2000, "Agent-Based Synthesis of Electromechanical Design Configurations," ASME J. Mech. Des., **122**(1), pp. 61–69.
[13] Münzer, C., Helms, B., and Shea, K., 2013, "Automatically Transforming Object-Oriented Graph-Based Representations Into Boolean Satisfiability Problems for Computational Design Synthesis," ASME J. Mech. Des., **135**(10), p. 101001.
[14] Silvas, E., Hofman, T., Murgovski, N., Etman, P., and Steinbuch, M., 2016, "Review of Optimization Strategies for System-Level Design in Hybrid Electric Vehicles," IEEE Trans. Veh. Technol., **PP**(99), (to be published).
[15] Liu, J., and Peng, H., 2010, "A Systematic Design Approach for Two Planetary Gear Split Hybrid Vehicles," Veh. Syst. Dyn., **48**(11), pp. 1395–1412.
[16] Zhang, X., Li, S. E., Peng, H., and Sun, J., 2015, "Efficient Exhaustive Search of Power-Split Hybrid Powertrains With Multiple Planetary Gears and Clutches," ASME J. Dyn. Syst., Meas., Control, **137**(12), p. 121006.
[17] Bayrak, A. E., Ren, Y., and Papalambros, P. Y., 2013, "Design of Hybrid-Electric Vehicle Architecture Using Auto-Generation of Feasible Driving Modes," ASME Paper No. DETC2013-13043.
[18] Bayrak, A. E., Ren, Y., and Papalambros, P. Y., 2014, "Optimal Dual-Mode Hybrid Electric Vehicle Powertrain Architecture Design for a Variety of Loading Scenarios," ASME Paper No. DETC2014-34897.
[19] Bayrak, A. E., Kang, N., and Papalambros, P. Y., 2015, "Decomposition-Based Design Optimization of Hybrid Electric Powertrain Architectures: Simultaneous Configuration and Sizing Design," ASME Paper No. DETC2015-46861.
[20] Kim, H. M., 2001. "Target Cascading in Optimal System Design," Ph.D. thesis, Department of Mechanical Engineering, University of Michigan, Ann Arbor, MI.
[21] Michelena, N., Park, H., and Papalambros, P. Y., 2003, "Convergence Properties of Analytical Target Cascading," AIAA J., **41**(5), pp. 897–905.
[22] Kang, N., Kokkolaras, M., and Papalambros, P. Y., 2014, "Solving Multiobjective Optimization Problems Using Quasi-Separable MDO Formulations and Analytical Target Cascading," Struct. Multidiscip. Optim., **50**(5), pp. 849–859.
[23] Kang, N., Kokkolaras, M., and Papalambros, P. Y., 2014, "Optimal Design of Commercial Vehicle Systems Using Analytical Target Cascading," Struct. Multidiscip. Optim., **50**(6), pp. 1103–1114.
[24] Tosserams, S., Etman, L., Papalambros, P., and Rooda, J., 2006, "An Augmented Lagrangian Relaxation for Analytical Target Cascading Using the Alternating Direction Method of Multipliers," Struct. Multidiscip. Optim., **31**(3), pp. 176–189.
[25] Bayrak, A. E., 2015, "Topology Considerations in Hybrid Electric Vehicle Powertrain Architecture Design," Ph.D. thesis, Department of Mechanical Engineering, University of Michigan, Ann Arbor, MI.
[26] Allison, J. T., and Herber, D. R., 2014, "Special Section on Multidisciplinary Design Optimization: Multidisciplinary Design Optimization of Dynamic Engineering Systems," AIAA J., **52**(4), pp. 691–710.
[27] Junkins, J., and Rew, D., 1988, "Unified Optimization of Structures and Controllers," *Large Space Structures: Dynamics and Control*, Springer, Berlin, pp. 323–353.
[28] Smith, M., Grigoriadis, K., and Skelton, R., 1992, "Optimal Mix of Passive and Active Control in Structures," J. Guid., Control, Dyn., **15**(4), pp. 912–919.
[29] Fathy, H. K., Reyer, J. A., Papalambros, P. Y., and Ulsoy, A. G., 2001, "On the Coupling Between the Plant and Controller Optimization Problems," American Control Conference, IEEE, Vol. 3, pp. 1864–1869.
[30] Peters, D. L., Papalambros, P. Y., and Ulsoy, A. G., 2015, "Relationship Between Coupling and the Controllability Grammian in Co-Design Problems," Mechatronics, **29**, pp. 36–45.
[31] Allison, J. T., Guo, T., and Han, Z., 2014, "Co-Design of an Active Suspension Using Simultaneous Dynamic Optimization," ASME J. Mech. Des., **136**(8), p. 081003.

Downloaded From: http://mechanicaldesign.asmedigitalcollection.asme.org/ on 06/03/2016 Terms of Use: http://www.asme.org/about-asme/terms-of-use

[32] Deodhar, N., Vermillion, C., and Tkacik, P., 2015, "A Case Study in Experimentally-Infused Plant and Controller Optimization for Airborne Wind Energy Systems," American Control Conference (ACC), IEEE, pp. 2371–2376.
[33] Fathy, H. K., Papalambros, P. Y., Ulsoy, A. G., and Hrovat, D., 2003, "Nested Plant/Controller Optimization With Application to Combined Passive/Active Automotive Suspensions," American Control Conference, IEEE, Vol. 4, pp. 3375–3380.
[34] Lin, C.-C., Peng, H., Grizzle, J. W., and Kang, J.-M., 2003, "Power Management Strategy for a Parallel Hybrid Electric Truck," IEEE Trans. Control Syst. Technol., **11**(6), pp. 839–849.
[35] Liu, J., and Peng, H., 2006, "Control Optimization for a Power-Split Hybrid Vehicle," American Control Conference, IEEE.
[36] Delprat, S., Guerra, T., and Rimaux, J., 2002, "Control Strategies for Hybrid Vehicles: Optimal Control," IEEE 56th Vehicular Technology, IEEE, Vol. 53, pp. 1681–1685.
[37] Kim, N., Cha, S., and Peng, H., 2011, "Optimal Control of Hybrid Electric Vehicles Based on Pontryagin's Minimum Principle," IEEE Trans. Control Syst. Technol., **19**(5), pp. 1279–1287.
[38] Paganelli, G., Delprat, S., Guerra, T.-M., Rimaux, J., and Santin, J.-J., 2002, "Equivalent Consumption Minimization Strategy for Parallel Hybrid Powertrains," IEEE 55th Vehicular Technology Conference VTC Spring 2002, IEEE, Vol. 4, pp. 2076–2081.
[39] Serrao, L., Onori, S., and Rizzoni, G., 2009, "ECMS as a Realization of Pontryagin's Minimum Principle for HEV Control," American Control Conference, IEEE, pp. 3964–3969.
[40] Cheong, K. L., Li, P. Y., and Chase, T. R., 2011, "Optimal Design of Power-Split Transmissions for Hydraulic Hybrid Passenger Vehicles," American Control Conference, IEEE, pp. 3295–3300.
[41] Antony, G. G., and Pantelides, A., 2006, "Precision Planetary Servo Gearheads," Technical Report No. 06FTM04, American Gear Manufacturers Association.

Downloaded From: http://mechanicaldesign.asmedigitalcollection.asme.org/ on 06/03/2016 Terms of Use: http://www.asme.org/about-asme/terms-of-use